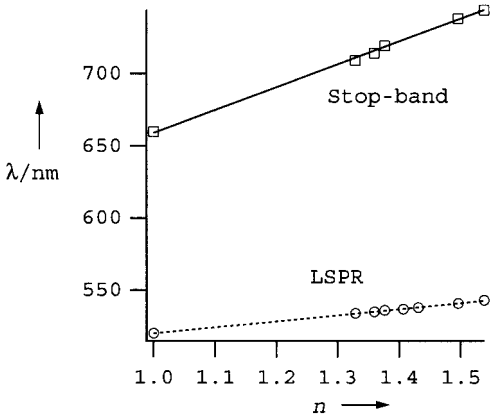

Figure 6. Dependence of the peaks originating from the LSPR (○) and the stop-band (□) on the refractive index. The dotted and solid lines were fitted by using linear functions.

ing from the LSPR can be clearly observed when the refractive index of the surrounding medium changes from 1 to 1.538. Hence, the LSPR can be used to determine any refractive index in this range. In summary, there are both merits and drawbacks to using the LSPR or stop-band peak alone to detect the surrounding medium, while a combination of the two peaks can give a more correct and precise result.

In conclusion, a high-quality metal-coated 3DOM was fabricated by a dipping method, and its application as a refractive index sensor was demonstrated. Both the LSPR and the stop-band can be used to measure the changes in the refractive index, and a combination of the two allows precise measurement of the refractive index of the surrounding medium over a wide range. Potential applications of this kind of film are as a biological sensor and as a vapor sensor. In addition, such a material may also have applications in surface-enhanced Raman scattering (SERS) and metal optical crystals.

Received: December 3, 2001 [Z18318]

[1] C. P. Collier, R. J. Saykally, J. J. Shiang, S. E. H. J. R. Henrichs, *Science* **1997**, *277*, 1978.
[2] C. B. Murray, C. R. Kagan, M. G. Bawendi, *Science* **1995**, *270*, 1335.
[3] R. F. Ziolo, E. P. Giannelis, B. A. Weinstein, M. P. O'Horo, B. N. Ganguly, V. Mehrotra, M. W. Russell, D. R. Huffmann, *Science* **1992**, *257*, 219.
[4] M. Zhao, L. Sun, R. M. Crooks, *J. Am. Chem. Soc.* **1998**, *120*, 4877.
[5] Y. S. Kang, S. Risbud, J. F. Rabolt, P. Stroeve, *Chem. Mater.* **1996**, *8*, 2209.
[6] T. S. Ahmadi, S. L. Logunov, M. A. El-Sayed, *J. Phys. Chem.* **1996**, *100*, 8053.
[7] A. Taleb, C. Petit, M. P. Pileni, *J. Phys. Chem. B* **1998**, *102*, 2214.
[8] J. Schmitt, P. Machtle, D. Eck, H. Möhwald, C. A. Helm, *Langmuir* **1999**, *15*, 3256.
[9] R. Elghanian, J. J. Storhoff, R. C. Mucic, R. L. Letsinger, C. A. Mirkin, *Science* **1997**, *277*, 1078.
[10] C. A. Mirkin, R. L. Letsinger, R. C. Mucic, J. J. Storhoff, *Nature* **1996**, *382*, 607.
[11] K. C. Grabar, P. C. Smith, M. D. Musick, J. A. Davis, D. G. Walter, M. A. Jackson, A. P. Guthrie, M. J. Natan, *J. Am. Chem. Soc.* **1996**, *118*, 1148.
[12] J. Schmitt, G. Decher, W. J. Dressick, S. L. Brandow, R. E. Geer, R. Shashidhar, J. M. Calvert, *Adv. Mater.* **1997**, *9*, 61.
[13] M. D. Malinsky, K. L. Kelly, G. C. Schatz, R. P. V. Duyne, *J. Am. Chem. Soc.* **2001**, *123*, 1471.
[14] J. C. Hulteen, D. A. Treichel, M. T. Smith, M. L. Duval, T. R. Jensen, R. P. V. Duyne, *J. Phys. Chem. B* **1999**, *103*, 3854.
[15] P. Jiang, J. F. Bertone, K. S. Hwang, V. L. Colvin, *Chem. Matter.* **1999**, *11*, 2132.
[16] Z.-Z. Gu, S. Hayami, S. Kubo, Q.-B. Meng, Y. Einaga, D. A. Tryk, A. Fujishima, O. Sato, *J. Am. Chem. Soc.* **2001**, *123*, 175.
[17] J. H. Fendler, *Nanoparticles and Nanostructured Films*, Wiley-VCH, New York, **1998**.
[18] Z.-Z. Gu, Q.-B. Meng, S. Hayami, A. Fujishima, O. Sato, *J. Appl. Phys.* **2001**, *90*, 2042.

A One-Dimensional BaI_2 Chain with Five- and Six-Coordination, Formed within a Single-Walled Carbon Nanotube**

Jeremy Sloan,* Sara J. Grosvenor, Steffi Friedrichs, Angus I. Kirkland, John L. Hutchison, and Malcolm L. H. Green

Single-walled carbon nanotubes (SWNTs)[1] are cylindrical sheets of sp^2 graphene carbon that, when formed by laser ablation[2] or arc vaporization,[3] form capillaries with diameters predominantly within the range of 1 to 2 nm. We have recently reported that one-dimensional (1D) crystals of rock-salt KI formed within these narrow capillaries exhibit a partial or total reduction in coordination.[4, 5] For example, a 1D KI crystal of 2×2 atomic layers formed within SWNTs 1.4 nm in diameter exhibits a total reduction from 6:6 (i.e., cation:anion) to 4:4 coordination.[4] Similarly, a 1D KI crystal of 3×3 atomic layers observed within wider SWNTs (1.6 nm in diameter) exhibits three separate coordinations of 6:6, 5:5, and 4:4 along central, face, and edge -I-K-I-K- rows, respectively.[5] Binary halides derived from layered or 3D polyhedral framework structures inserted into SWNTs form 1D polyhedral chain structures[6] that also exhibit reduced cation and anion coordination. For example, six-coordinate

[*] Dr. J. Sloan, S. J. Grosvenor, S. Friedrichs, Prof. M. L. H. Green
Inorganic Chemistry Laboratory
University of Oxford
South Parks Road, Oxford OX1 3QR (UK)
Fax: (+44) 1865-272690
E-mail: jeremy.sloan@chem.ox.ac.uk
Dr. J. L. Hutchison
Department of Materials
University of Oxford
Parks Road, Oxford OX1 3PH (UK)
Dr. A. I. Kirkland
University of Cambridge
Department of Materials Science and Metallurgy
Pembroke Street, Cambridge CB2 3QZ (UK)

[**] The authors acknowledge financial support from the Petroleum Research Fund, administered by the American Chemical Society (Grant No. 33765-AC5), the EPSRC (Grant Nos. GR/L59238 and GR/L22324) and Colebrand Ltd. Additionally, J.S. is indebted to the Royal Society for a University Research Fellowship, while S.F. is indebted to BMBF and to Fonds der Chemischen Industrie.

  1433-7851/02/4107-1156 $ 20.00+.50/0

Cd^{2+} in $CdCl_2$ and nine-coordinate Tb^{3+} in $TbCl_3$ form five- and six-coordinate 1D zigzag polyhedral chains within SWNTs, respectively.[7, 8] While both these structures form with a reduced rearranged anion sublattice, they retain effectively the cation sublattice of the corresponding bulk halides. Here we report the first example of a 1D crystal chain derived from an alkaline earth metal halide (BaI_2) for which both sublattices are substantially different from those found in any of the published forms of the bulk halide.

BaI_2 is one of a group of dihalides that adopt the nine-coordinate *Pnam* cotunnite $PbCl_2$ structure under standard conditions[9] but which transforms into a hexagonal $P\bar{6}2m$ form under 3 GPa pressure[10] and a 10-coordinate post-cotunnite monoclinic $P112_1/a$ form between 5 and 15 GPa pressure.[11] The *Pnam* and $P\bar{6}2m$ forms both consist of a 3D network of face-sharing distorted tricapped trigonal prisms (Figure 1a and b), the major difference being that, for the latter, the I^- coordination is more symmetrical. The highest pressure version consists of a network of tetracapped trigonal prisms (Figure 1c) and, together with the *Pnam* and $P\bar{6}2m$ forms, these are the only coordinations reported for Ba^{2+} within BaI_2.

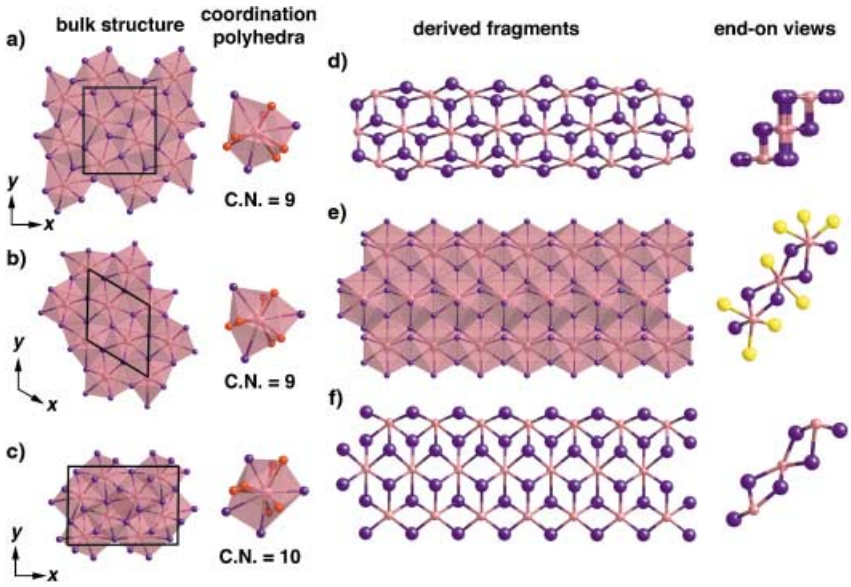

Figure 1. a) Cotunnite *Pnam* form of BaI_2. b) Hexagonal $P\bar{6}m$ modification of BaI_2 formed under 3 GPa pressure. c) 10-coordinate $P112_1/a$ form of BaI_2 formed between 5 and 15 GPa pressure. d) Staggered view and end-on representation of a 1D BaI_2 chain incorporated in a SWNT. e) Side-on and end-on views of the fragment which can be defined along *z* for both the *Pnam* and $P\bar{6}m$ forms. The net stoichiometry of the structure can be restored to BaI_2 by removing the iodine atoms marked yellow (end-on view). f) Side-on and end-on views of reduced-coordination BaI_2 fragment. C.N. = coordination number.

A sample of SWNTs was prepared by a catalytic arc-synthesis route[12] and filled with BaI_2 by capillary wetting.[13, 14] The composite was examined in a 300-kV high-resolution (HR) field emission gun transmission electron microscope (FEGTEM). Lattice images showed that only 10–20% of the SWNTs contained filling, which was predominantly crystalline but also very sensitive to the electron beam, with the result that it became glassy after irradiation at a beam dosage of $5 \times 10^5\ e^-\,nm^{-2}\,s^{-1}$ for longer than about 20 s. Single HRTEM images were therefore obtained from the crystals in conventional imaging mode with low electron beam dosages ($2 \times 10^5\ e^-\,nm^{-2}\,s^{-1}$). Even under these conditions, it was not possible to use the previously described focal series restoration approach[5, 15] to image the specimen.

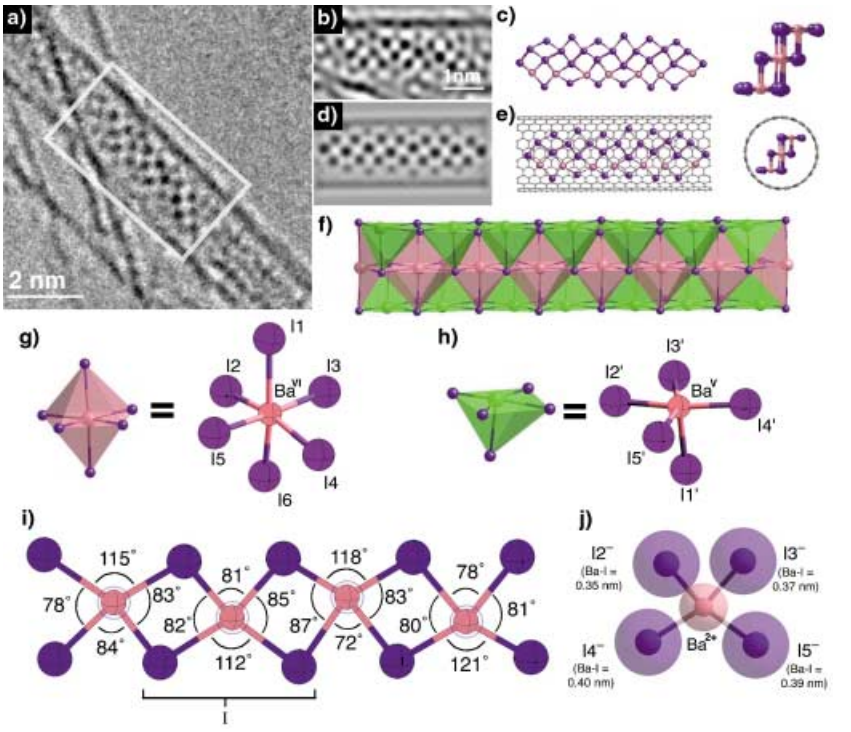

Figure 2. a) HRTEM image of BaI_2/SWNT composite. b) Detail from boxed region in (a), for which image noise was reduced with a deconvolution filter. c) Structure plot based on a 2D peak-mapping analysis of (b); end-on view on the right. d) Simulated HRTEM image, e) complete structure model of BaI_2/SWNT composite. f) Coordination model of 1D BaI_2 chain. g) 5-coordinate, h) 6-coordinate BaI_6 polyhedra and ball-and-stick models derived from (c). i) and j) Models showing derived equatorial bond angles and distances for BaI_4 units along the center of the 1D BaI_2 chain (ionic radii in (j) indicated by diffuse spheres).

An image and the corresponding detail, obtained close to ideal Scherzer HRTEM focusing conditions, of a BaI_2-filled SWNT 1.6 nm in diameter overlying two unfilled SWNTs are shown in Figure 2a and b. The microstructure of the filling material is clearly visible as a 2D array of dark spots which are lighter in intensity close to the walls of the SWNT and heavier in intensity towards its center. As the electron-scattering power of Ba ($Z = 56$) is similar to that of I ($Z = 53$) we assume that the dark spots correspond to columns 1–3 atoms thick in projection, each of which may contain some combination of Ba and I. The columnar spacings in the fragment were typical of those observed in other BaI_2-

  1433-7851/02/4107-1157 $ 20.00+.50/0

filled SWNTs, and we believe that the crystal microstructure is therefore representative, although the microstructure of SWNT fillings is known to vary as a function of tube diameter.[4, 5, 8]

To construct a model for the encapsulated crystal, a 2D peak-mapping program was used to determine the relative positions of the atomic columns in Figure 2b, and this produced the atom map shown in Figure 2c. To derive the complete crystal, the fragment was expanded vertically with respect to the plane of the page to give the end-on representation shown on the right of Figure 2c, in which the fragment can be visualized as being 1-2-3-2-1 atomic layers in thickness. Atomic positions were assigned on the basis of a coordination scheme for Ba and I which retains Ba in the +2 oxidation state. The vertical expansion was scaled to take into account the Ba–I bond length anticipated from the ionic radii of Ba^{VI2+} (0.136 nm)[16] and I^{VI-} (0.22 nm),[16] that is, 0.356 nm. A near-Scherzer focus simulated HRTEM image[4] (Figure 2d), calculated from a composite crystal consisting of a 4 nm long section of a (12,12) SWNT[17] and the derived crystal fragment (Figure 2e), provides good agreement with the experimental image. An end-on view of the composite is shown on the right of Figure 2e. A coordination polyhedra model derived from the 1D chain (Figure 2f) produces octahedral coordination for the Ba^{2+} ions along the center of the chain and pentagonal coordination for the Ba^{2+} ions on the edges of the chain (see also Figure 2g and h).

By combining information from the lattice image and the structural model, it is possible to derive information regarding I-Ba-I bond angles and distances within the 1D BaI_2 crystal. The equatorial I-Ba-I bond angles can be estimated from the spot dispositions in the lattice image (Figure 2b), as shown schematically for the representative fragment in Figure 2i. The apical Ba–I distances must be estimated from the ionic radii of Ba^{2+} and I^- (see above). The equatorial Ba–I distances can be estimated from the intercolumnar distances measured from the dark spots in the micrograph, and this gives values ranging from 0.35 to 0.40 nm (estimated error ±0.02 nm), as shown for the representative polyhedra in Figure 2j. Any out-of-plane distortions will cause these distances to be longer, by inspection. Such expansions notwithstanding, the estimated Ba–I distances are either equal to or slightly longer than the apical Ba–I distance of 0.356 nm predicted from the ionic radii (see above). The close correspondence of these measured values with the predicted bond lengths is an important argument in favor of our model.

An exhaustive comparison of the experimental structure (shown in perspective view in Figure 1d) and all possible fragments derived from the structures in Figure 1a–c could only produce one approximate match with the experimental structure, shown in Figure 1e. Versions of this fragment can be derived from either the *Pnam* or $P\bar{6}m$ forms of BaI_2 (Figure 1a and b), although both have an excess of iodine due to lattice termination. It is therefore necessary to remove the atoms depicted in yellow in Figure 1e to restore the stoichiometry to BaI_2 (see Figure 1f). While this structure resembles that of the experimental fragment (Figure 1d), comparison of the end-on views of the two fragments reveals that the similarity is only superficial. The Ba^{2+} ions exist in a far more compressed environment in the experimental fragment than in the derived fragment (cf. end-on views in Figure 1d and f). The extent of this difference is reflected in two key experimental observations: 1) the shortening of the Ba–Ba distance defined along diagonally related BaI_x polyhedra from 0.597 (*Pnam* form) or 0.588 ($P\bar{6}m$ form) to 0.49 nm; 2) the much more symmetrical coordination of iodine in the 1D chain. We conclude that the experimental 1D fragment has a crystal structure substantially different to any of the reported forms of BaI_2.

This work describes the structural characterization of a BaI_2 nanocrystal formed within a SWNT of 1.6 nm diameter by using a "bottom-up" approach. The obtained structure is found to have Ba in 5- and 6-coordination—both unknown in bulk BaI_2—in the form of a 1D chain consisting of edge-linked coordination polyhedra. This result represents a significant departure from those for previously described SWNT fillings,[1–3] as it represents the first example for which all structural properties of an SWNT-encapsulated crystal are different from those of the bulk structure. It is anticipated that the physical properties of the derived 1D chain will be substantially modified as a result.

Experimental Section

A sample of as-prepared SWNTs, prepared according to a published catalytic arc-synthesis method,[12] and a sample of highly pure anhydrous BaI_2 (Aldrich, 99.999%) were combined in 1:1 mass ratio. The mixture was ground using a pestle and mortar and then transferred to a silica quartz tube 6 mm in diameter. This procedure was performed under dry conditions in a glove box, due to the deliquescent nature of BaI_2. The quartz tube was then sealed under vacuum. The ampoule was heated at 1 K min^{-1} to 40 K above the melting temperature of the salt (i.e., 740 °C) and held at this temperature for 5 h. The furnace was set to a slow cooling program (from 780 to 18 °C over 1 h) to allow for optimum growth of the salt crystals within the SWNTs.

The product was examined in a 300-kV JEOL JEM-3000F field emission gun HRTEM (point resolution 0.16 nm) equipped with a LINK "ISIS" X-ray microanalysis system. Images were acquired digitally on a Gatan model 794 (1 k × 1 k) CCD camera, the magnification of which was calibrated with Si[110] lattice spacings. Energy dispersive X-ray microanalysis (EDX) was performed with a electron probe 0.5 nm in diameter. Image simulations were performed by using a standard multislice algorithm incorporating representative parameters for our FEGTEM.

Received: November 15, 2001 [Z18221]

[1] a) S. Iijima, T. Ichihashi, *Nature* **1993**, *363*, 603–605; b) D. S. Bethune, C. H. Kiang, M. S. de Vries, G. Gorman, R. Savoy, J. Vazquez, R. Beyers, *Nature* **1993**, *363*, 605–607.

[2] P. M. Ajayan, J. M. Lambert, P. Bernier, L. Barbedette, C. Colliex, J. M. Planeix, *Chem. Phys. Lett.* **1993**, *215*, 509–517.

[3] T. Guo, P. Nikolaev, A. Thess, D. T. Colbert, R. E. Smalley, *Chem. Phys. Lett.* **1995**, *243*, 49–54.

[4] J. Sloan, M. C. Novotny, S. R. Bailey, G. Brown, C. Xu, V. C. Williams, S. Friedrichs, E. Flahaut, R. L. Callendar, A. P. E. York, K. S. Coleman, M. L. H. Green, R. E. Dunin-Borkowski, J. L. Hutchison, *Chem. Phys. Lett.* **2000**, *329*, 61–65.

[5] R. R. Meyer, J. Sloan, R. E. Dunin-Borkowski, A. I. Kirkland, M. C. Novotny, S. R. Bailey, J. L. Hutchison, M. L. H. Green, *Science* **2000**, *289*, 1324–1326.

[6] J. Sloan, M. L. H. Green in *Fullerenes: Chemistry, Physics and Technology* (Eds.: K. M. Kadish, R. S. Ruoff), Wiley Interscience, New York, **2000**, pp. 795–838.

  1433-7851/02/4107-1158 $ 20.00+.50/0

[7] J. Sloan, G. Brown, S. R. Bailey, K. S. Coleman, E. Flahaut, S. Friedrichs, C. Xu, M. L. H. Green, R. E. Dunin-Borkowski, J. L. Hutchison, A. I. Kirkland, R. R. Meyer, *Proceedings of the MRS* **2001**, *633*, A14.31/1 – A14.31/6.
[8] C. Xu, J. Sloan, G. Brown, S. R. Bailey, V. C. Williams, S. Friedrichs, K. S. Coleman, E. Flahaut, J. L. Hutchison, R. E. Dunin-Borkowski, M. L. H. Green, *Chem. Commun.* **2000**, 2427 – 2428.
[9] E. B. Brackett, T. E. Brackett, *J. Phys. Chem.* **1963**, *67*, 2132 – 2135.
[10] H. P. Beck, *J. Solid State Chem.* **1983**, *47*, 328 – 332.
[11] J. M. Léger, J. Haines, A. Atouf, *J. Appl. Crystallogr.* **1995**, *28*, 416 – 423.
[12] C. Journet, W. K. Maser, P. Bernier, A. Loiseau, M. Lamy de la Chapelle, S. Lefrant, P. Derniard, J. E. Fisher, *Nature* **1997**, *388*, 756 – 758.
[13] J. Sloan, D. M. Wright, H. G. Woo, S. Bailey, G. Brown, A. P. E. York, K. S. Coleman, J. L. Hutchison, M. L. H. Green, *Chem. Commun.* **1999**, 699 – 700.
[14] P. M. Ajayan, S. Iijima, *Nature* **1993**, *361*, 333 – 334.
[15] S. Friedrichs, J. Sloan, M. L. H. Green, J. L. Hutchison, R. R. Meyer, A. I. Kirkland, *Phys. Rev. B* **2001**, *64*, DOI 045406/1-045406/8.
[16] R. D. Shannon, *Acta Crystallogr. Sect. A* **1976**, *32*, 751 – 767.
[17] M. S. Dresselhaus, G. Dresselhaus, R. Saito, *Carbon* **1991**, *33*, 883 – 891.

Rational Design of Homochiral Solids Based on Two-Dimensional Metal Carboxylates**

Yong Cui, Owen R. Evans, Helen L. Ngo, Peter S. White, and Wenbin Lin*

The design and construction of metal – organic coordination networks (MOCNs) have received significant attention in recent years, mostly motivated by the potential of generating tailor-made functional materials through molecular engineering of the constituent building blocks using the tools of modern synthetic chemistry.[1] Indeed many MOCNs have been reported to exhibit interesting properties, which include functional-group or size-selective sorption,[2] catalysis,[3] gas storage,[4] molecular recognition,[5] and second harmonic generation.[6] Among these, the synthesis of MOCNs with permanent porosity is by far the most fruitful, and many metal – carboxylate coordination networks with extremely large surface areas have been constructed, based on the secondary building unit (SBU) concept that has been extensively used in zeolite synthesis.[7] Compared to zeolites and the recently developed MCM-type mesoporous materials, MOCNs are built with weaker metal – ligand coordination bonds and are inherently less stable. It is thus imperative to incorporate functions that are not possible with inorganic oxide materials into MOCNs. Our recent success with crystal engineering of nonlinear-optical (NLO) materials based on MOCNs provides such an example.[6] Another unique feature of MOCNs is the ability to design chiral pores and functionalities, which may be exploited in heterogeneous asymmetric catalysis and enantioselective separations.[8] With a few exceptions,[3b,c, 9] the chiral MOCNs reported to date were synthesized from simple achiral components.[10] The chirality of such MOCNs originates from the spatial disposition of their building blocks and is not amenable to fine tuning.[1d] Moreover, the bulk materials of such MOCNs tend to be racemic and cannot be exploited for chirotechnology.[11] A more straightforward approach to chiral solids relies on the use of metal ions or metal clusters as nodes, and chiral multifunctional ligands to link these nodes. Herein we report the rational synthesis of chiral two-dimensional (2D) networks, based on enantiopure dicarboxylate bridging ligands and metal – organic SBUs.

As illustrated in Scheme 1, enantiopure atropisomeric 6,6′-dichloro-2,2′-diethoxy-1,1′-binaphthylene-4,4′-dicarboxylic acid (H_2BDA), was prepared in six steps in good overall yield (35.7 %), from the readily available chiral 1,1′-bi-2-naphthol (BINOL). Homochiral metal carboxylates with the general formula of $[M_2(\mu\text{-}H_2O)(bda)_2(py)_3(dmf)]\cdot(DMF)\cdot(H_2O)_x$ (M = Mn, $x = 2$, **1a**; M = Co, $x = 3$, **1b**; M = Ni, $x = 3$, **1c**) were obtained in moderate yields (31 – 42 %), by treatment of metal nitrate or perchlorate salts with H_2BDA in a mixture of N,N'-dimethylformamide (DMF), MeOH, and pyridine (py) at 60 °C (Scheme 2). Compounds **1a** – **c** are stable in air, and insoluble in water and common organic solvents. The IR spectra of **1a** – **c** exhibited bands at 1660 – 1320 cm^{-1} characteristic of carboxylate groups. Thermogravimetric analyses (TGA) show that **1a** loses 12.8 % of its total weight on heating to 220 °C, which corresponds to the loss of three water molecules and two DMF molecules per formula unit (expected 12.7 %). TGA indicate that **1b** and **1c** experience 13.7 % and 13.3 % weight losses by 220 °C, corresponding to the loss of four water molecules and two DMF molecules for both **1b** and **1c** (expected 13.9 %). The formulations of **1a** – **c** are supported by microanalysis results.

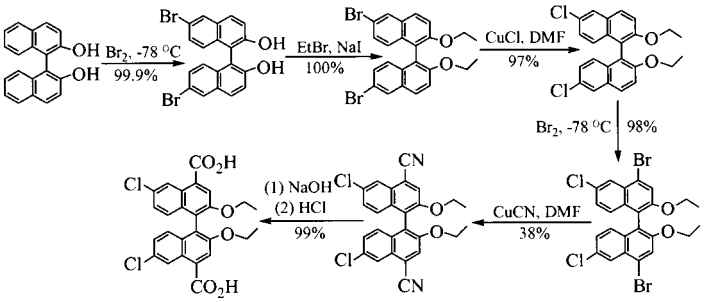

Scheme 1. Synthesis of 6,6′-dichloro-2,2′-diethoxy-1,1′-binaphthylene-4,4′-dicarboxylic acid (H_2BDA).

[*] Prof. W. Lin, Dr. Y. Cui, O. R. Evans, H. L. Ngo, Dr. P. S. White
Department of Chemistry, CB#3290
University of North Carolina, Chapel Hill, NC 27599 (USA)
Fax: (+1) 919-962-2388
E-mail: wlin@unc.edu

[**] We acknowledge financial support from NSF (DMR-9875544). We thank Dr. Gary Enright for the X-ray powder diffraction patterns. W.L. is an Alfred P. Sloan Fellow, an Arnold and Mabel Beckman Young Investigator, a Cottrell Scholar of Research Corp, and a Camille Dreyfus Teacher-Scholar.

Supporting information for this article is available on the WWW under http://www.angewandte.com or from the author.

  1433-7851/02/4107-1159 $ 20.00+.50/0